ELSEVIER

Polymer 41 (2000) 8121–8138

polymer

www.elsevier.nl/locate/polymer

Thermal stability, crystallization kinetics and morphology of a new semicrystalline polyimide based on 1,3-bis(4-aminophenoxy) benzene and 3,3′,4,4′-biphenyltetracarboxylic dianhydride

V. Ratta[a], A. Ayambem[b], R. Young[a], J.E. McGrath[b], G.L. Wilkes[a,*]

[a]*Department of Chemical Engineering, NSF Science and Technology Center for High Performance Polymeric Adhesives and Composites, Virginia Tech, Blacksburg, VA 24061, USA*

[b]*Department of Chemistry, NSF Science and Technology Center for High Performance Polymeric Adhesives and Composites, Virginia Tech, Blacksburg, VA 24061, USA*

Received 10 December 1998; received in revised form 28 January 2000; accepted 31 January 2000

Abstract

This work investigates the crystallization kinetics and thermal stability of a new melt processable semicrystalline polyimide (T_g = 210°C, T_m = 395°C) based on 1,3-bis(4-aminophenoxy) benzene and 3,3′,4,4′-biphenyltetracarboxylic dianhydride, and endcapped with phthalic anhydride. Earlier studies have demonstrated that this polymer is a strong candidate as a structural adhesive for high-temperature and high-performance applications. In this study, an Avrami Analysis was utilized to study the bulk crystallization kinetics as a function of crystallization temperature, melt time and melt temperature. For the crystallization temperatures studied, the Avrami parameter *K* increased substantially for small increases in undercooling or small decreases in melt temperature and residence time. Spherulitic growth rates were measured microscopically at different crystallization temperatures. The effect of varying the melt time and temperature on the growth rate at a particular temperature was determined. The variation in the Avrami parameters is correlated with independent microscopic observations of the nucleation density and the spherulitic growth rates.

Melt viscosity was followed as a function of melt temperature, residence time in the melt and deformation rate. Higher melt temperatures result in a faster increase in the isothermal melt viscosity indicating chemical changes in the polymer at such high melt temperatures. Followed rheologically, onset of crystallization requires greater undercooling when cooling from higher melt temperatures. Non-isothermal crystallization was followed using DSC and optical microscopy, both of which gave evidence of a distinct 'catastrophic nucleation' process at temperatures in the vicinity of 330°C during cooling from the melt.

Keywords: Thermal stability; Crystallization kinetics; Semicrystalline polyimide

1. Introduction

Aromatic polyimides are an important subset of high-performance and high-temperature polymers which, due to their outstanding properties, are finding increasing use in applications such as high-temperature adhesives, composites, electronics packaging, fibers, foams and as membranes for gas separation [1,2]. Semicrystallinity in these polyimides further improves certain mechanical properties [3], thermal stability [4,5], radiation [6] and chemical resistance [7]. However, of the relatively few semicrystalline polyimides available, most rapidly lose their crystallization ability once taken to the required melt temperature, which is often in excess of 380°C. Melt relative to solution processing of these high-performance polymers is thought desirable both from an environmental standpoint (to avoid toxic solvents) and also for ease of processing. Recently, a new polyimide was developed in our laboratory that has displayed excellent characteristics from this standpoint. This polyimide (T_g = ca. 210°C, T_m^o = 395°C) is based on 1,3-bis(4-aminophenoxy) benzene (TPER diamine or 1,3(4)APB) and 3,3′,4,4′-biphenyltetracarboxylic dianhydride (BPDA) [4,5,8] (Scheme 1). It was also very important to fully endcap the chains with phthalic anhydride (PA) to maximize thermal stability [5]. Earlier DSC melting studies in our laboratories have demonstrated the excellent thermal stability of this polyimide by showing that very little change in the melting behavior occurred, even after 20 min at 430°C [4,5]. Previous study has also shown the outstanding adhesion properties of this polyimide to titanium alloy, e.g. average lap-shear strengths of

* Corresponding author. Tel.: + 1-540-231-5498; fax: + 1-540-231-9511.

0032-3861/00/$ - see front matter
PII: S0032-3861(00)00125-7

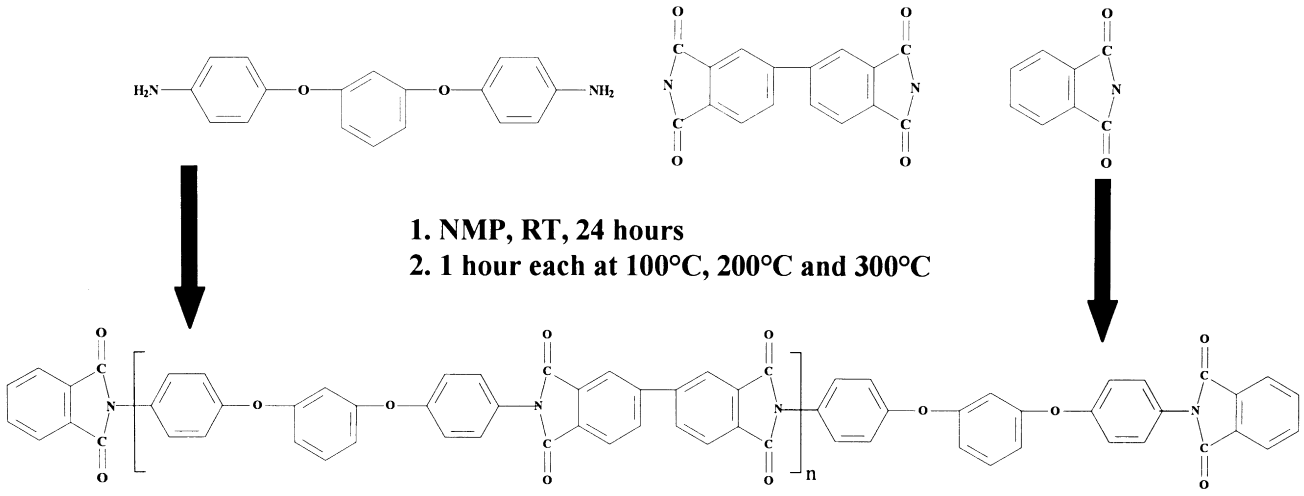

Scheme 1.

6600–8400 psi (46–59 MPa) at ambient temperatures, which compared favorably with the highest such strengths reported for any adhesive in literature. The adhesive bonds were also stable to a variety of solvents, high-temperature aging and elevated test temperatures of 177 and 232°C [4].

However, for such high-temperature thermoplastic polymers processed from the melt, melt time and temperature become important variables from processing and thermal stability viewpoints. Side reactions like crosslinking, branching or chain scission, that may occur at these high melt temperatures usually lead to build up in the molecular weight, and will not only change the rheolgical behavior but may also result in reduced crystallinity and slower crystallization kinetics. On the positive side, the rise in the molecular weight usually leads to improvement of certain mechanical properties, like higher elongation to break and increased toughness. Thus if the rise in molecular weight can be limited to an extent, such that the crystallization kinetics and the amount of crystallinity are not greatly affected, then a synergistic effect can be produced. In order to obtain this synergism however, it is important to evaluate the rheological behavior at these melt temperatures and the crystallization response when the polyimide is cooled from these harsh melt conditions. The effect of various melt conditions on the subsequent crystallization response also serves as a direct tool in evaluating the thermal stability of the system.

This paper examines some of these later-mentioned issues, such as the effect of melt holding conditions on isothermal crystallization kinetics and on the related morphology, in detail. An Avrami analysis of the DSC and corresponding polarized optical microscopy (POM) data were utilized to understand the effect of (1) crystallization temperature, (2) melt time and (3) melt temperature on the crystallization kinetics and the resulting morphology of the system.

Melt viscosity studies were conducted at various temperatures to detect the presence of any chemical changes and to ascertain the effect on subsequent crystallization. Non-isothermal studies were also performed using the DSC and hot stage POM to understand the effect of previous melt holding conditions on the subsequent crystallization behavior and semicrystalline morphology of the polyimide.

2. Experimental

The details specifying the synthesis of this polymer has been described elsewhere [3,4]. This study, however, will only utilize $M_n = 15,000$ Da ($M_w = 30,000$ Da) molecular weight version of this polymer which facilitates a low melt viscosity, and yet is high enough to demonstrate good physical behavior. POM was performed on a Zeiss optical microscope equipped with a Linkam 600 hot stage, a 35 mm camera and a video camera. The hot stage was calibrated using melting point standards and all experiments were conducted under a nitrogen purge. The spherulitic growth-rate measurements were performed on thin films (ca. 50 μm) sandwiched between two microscope cover slips. The samples were rapidly heated (ca. 90°C/min) to various melt temperatures and quenched to the desired crystallization temperature (within 15 s) using a separate nitrogen source. The growth of spherulites was measured as function of time using a Boeckeler video measurement system. Measurements were performed on four to six spherulites in a given sample and the average is reported. DSC experiments for both isothermal and non-isothermal crystallization were performed on a Perkin–Elmer DSC-7. The amount of polymer utilized in a given thermal scan was kept between 6–8 mg. The DSC was calibrated with indium and zinc standards. All experiments were conducted under a nitrogen purge and a DSC baseline was determined by running empty pans. For isothermal crystallization experiments, the samples were kept at room temperature and

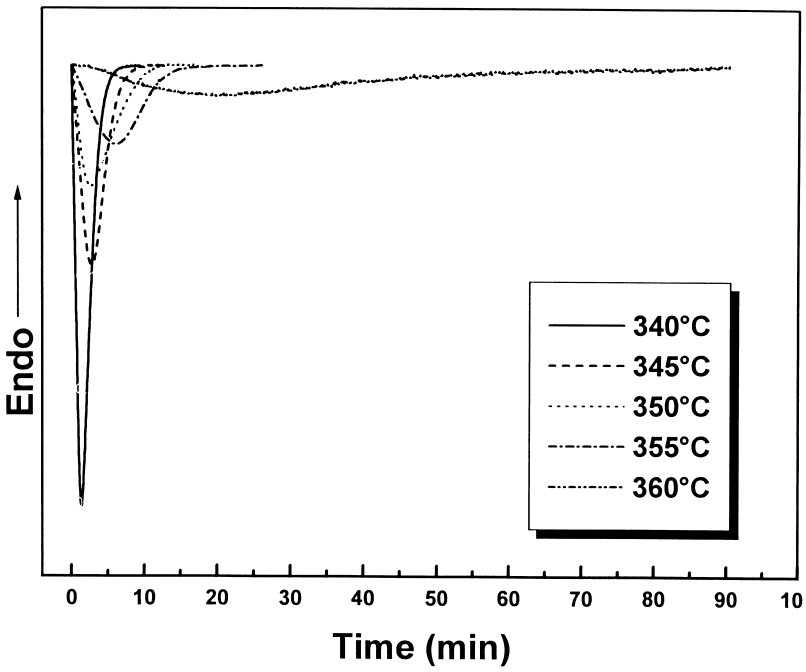

Fig. 1. Crystallization exotherms at various crystallization temperatures after 20 min residence time at 430°C.

purged with nitrogen for 5 min to remove air from the DSC cell. The samples were then rapidly heated to the desired melt temperatures and kept at that temperature for the desired amount of time. Cooling from these melt temperatures to specific crystallization temperatures was conducted at 200°C/min. In this regard, data collection at high supercoolings was hampered by the initial instability of the DSC signal. This initial instability occurs on cooling to the crystallization temperature at fast cooling rates and may persist for ca. 1 min on our Perkin–Elmer DSC 7. At higher supercooling, the induction times are short and crystallization is so fast that it is nearly over before the DSC signal has equilibrated. To obtain the initial portion of the exotherm at these temperatures, the straight-line region extending from the beginning of the exotherm was extrapolated to the horizontal baseline drawn from the end of the exotherm. The intersection of these two lines was taken as the start of the crystallization exotherm. Such a procedure was attempted for higher degrees of supercooling only when a sufficient straight-line portion of the initial exotherm was available. Rheological measurements were performed using a Rheometrics RMS-800 rheometer equipped with a 25 mm parallel plate tooling. The experiments were conducted in a nitrogen environment using 5% strain and 1.6 mm gap between the plates. The polymer film (1.5 g) was compacted at 300°C under a pressure of more than 20 MPa to yield circular discs. These discs were inserted between the circular plates of the rheometer, which were already preheated to the designated temperature. Although the temperature usually decreased 20–30°C while inserting the samples, the predetermined temperature was again quickly attained by fast heating. The data was collected from the time the material reached the desired temperature; these time-sweep experiments were conducted at temperatures of 410, 420, 430, 440 and 450°C for a period of 20 min at a frequency of 1 rad/s. To observe the rheology of supercooled melts, all the samples used for time-sweep experiments were cooled at a rate of 10°C/min while the percent strain and frequency were unchanged. These tests were stopped after crystallization of the sample was observed and the torque had exceeded 500 g cm. Tests were also conducted to examine the change in complex viscosity when the angular frequency was varied from 0.1 to 100 rad/s while keeping the strain amplitude constant at 5% and the temperature at 430°C. Viscosity at the highest frequency was measured first while the lowest frequency was determined last. It took ca. 8 min for one such isothermal 'frequency sweep' while four such consecutive sweeps were carried out on the same sample.

3. Results and discussion

Although the various experimental [9] and theoretical complications [10–13] associated with the traditional isothermal Avrami analysis are well recognized, it continues to be the most widely used means of describing the overall bulk isothermal crystallization of polymers. Also, its use together with direct morphological information using microscopy yields important information about the crystallization mechanism and kinetics of a given polymer. In this regard, the Avrami equation is generally written as:

$$X_c(t) = 1 - \exp(-Kt^n) \quad (1)$$

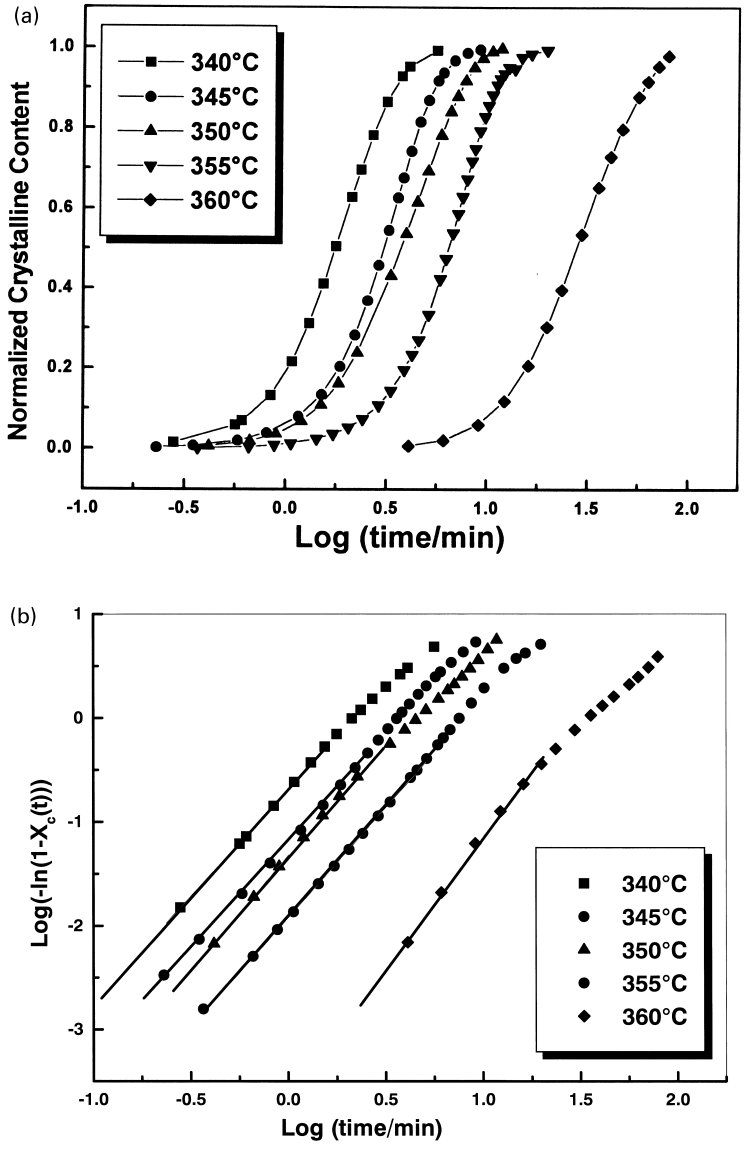

Fig. 2. (a) Normalized crystalline content as a function of log(t) at various crystallization temperatures. (b) Avrami plot of log[$-ln(1 - X_c(t))$] versus log(t) at various crystallization temperatures.

Isothermal DSC is the primary means of performing such an analysis, where $X_c(t)$, the normalized crystalline content at time t is written as:

$$X_c(t) = \Delta H(t)/\Delta H(\infty) \tag{2}$$

where $\Delta H(t)$ is the fractional heat of fusion after crystallization time t and $\Delta H(\infty)$ the total heat of crystallization observed at that isothermal crystallization temperature. K and n are Avrami constants and are indicative of the crystallization mechanisms involved. The exponent n in the Avrami equation can provide information on nucleation type and crystal growth geometry. K is dependent upon the dimensionality of the growing crystalline entities (e.g. whether they are spheres, discs or rods), as well as the type and amount of nucleation (sporadic or predetermined) and the linear growth rate G of the growing crystalline moieties. For example, in case of three-dimensional predetermined spherulitic crystallization K can be expressed as:

$$K = (4\Pi/3)N_o G^3 \tag{3}$$

Here N_o is the nucleation density whereas the exponent of 3 on the growth-rate term indicates the Avrami exponent for such a process. The parameters in Eq. (1) are usually determined by taking the double logarithm of Eq. (1) and expressing it in the form:

$$\log[-\ln(1 - X_c(t))] = \log K + n \log t \tag{4}$$

Fig. 1 shows the crystallization exotherms for TPER–BPDA–PA ($M_n = 15,000$ Da) after quenching from the melt to various crystallization temperatures. As is clearly

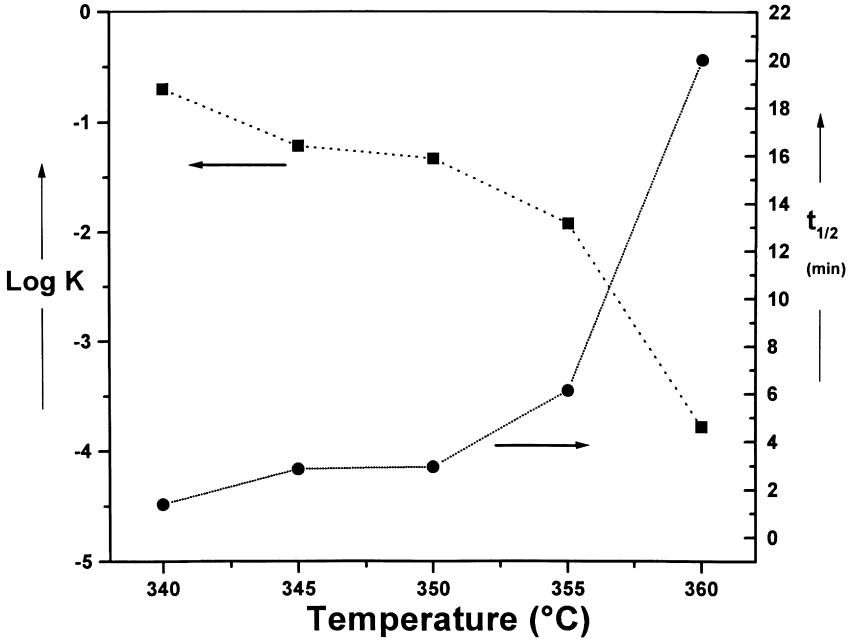

Fig. 3. Variation of logarithm of transformation rate K and crystallization half time $t_{1/2}$, as a function of crystallization time after melt holding conditions of 430°C for 20 min.

evident, the overall bulk crystallization is very temperature sensitive in the narrow 20°C range of 340–360°C. Although the rate of crystallization at 360°C is slow as evidenced by a broad crystallization exotherm, an increase in the degree of supercooling by 20°C leads to a large increase in the rate of crystallization. This change in rate of bulk crystallization is reflected in the crystallization half-time ($t_{1/2}$), the time to complete 50% of the total crystallization, which decreases from ca. 20 min at 360°C to 1.38 min at 340°C. At crystallization temperatures higher than 360°C, the crystallization is very slow and the exothermic signal approaches the sensitivity of DSC making collection of reliable data difficult. Collection of isothermal data below 340°C was not possible as the crystallization half time at those temperatures is less than the time it takes for the DSC signal to become stable (ca. 1 min). Crystallization of this polyimide (M_n = 11,500 Da) has also been studied by Hsiao et al. [14] who determined a $t_{1/2}$ time of 12 s at 350°C after cooling at 320°C/min from a less stringent initial melt condition of 420°C for 10 min. Although the effects of initial melt history on $t_{1/2}$ are discussed later in this paper, it is important to point out that these conclusions by Hsiao et al. are believed to be in question. While it is not clear how they measured such a short $t_{1/2}$ (the initial instability in the DSC signal itself always lasts for much more than 12 s), it is also surprising that they indicate three $t_{1/2}$ data points below the glass transition temperature (T_g of 220°C as indicated in their paper).

Fig. 2(a) shows the normalized crystalline content as a function of log (time) for the crystallization temperatures examined in this study. It is observed that the crystallization kinetics shifts to longer times with every 5°C increase in the crystallization temperature, this shift to longer times being most noticeable between 355 and 360°C. Fig. 2(b) shows the corresponding Avrami plots for the various crystallization temperatures. The curves show an initial linear section but a change in the slope is observed at longer times. The straight-line fit through the initial section of the curves, however, yields the two important Avrami parameters, K and n. The variation of bulk transformation rate K and the corresponding changes in crystallization half-time $t_{1/2}$ (which is a measure of the rate of crystallization), with crystallization temperature are shown in Fig. 3. A strong correlation between the value of parameter K and $t_{1/2}$ is observed with $t_{1/2}$ decreasing with increasing values of K.

Fig. 4 shows the optical micrographs taken at various crystallization temperatures, the initial melt conditions being identical to the DSC experiments described above. While the nucleation density is low at 355°C, it increases sharply with small increases in the degree of supercooling. Thus it is evident that the final spherulitic size decreases greatly with relatively small changes in the crystallization temperature. In fact, no optically resolvable spherulites were observed at and below 330°C due to a catastrophic increase in the nucleation density. This phenomenon will be addressed later in the paper. A small but noticeable change in the Avrami exponent is also observed with varying crystallization temperature. The Avrami exponent is 2.7 at 360°C whereas it decreases to 2.0 at 345 and 340°C. However, for spherulitic crystallization and a somewhat mixed mode of nucleation observed, the value of the Avrami exponent is expected to be slightly above 3. This may be because the Avrami exponent is calculated using the

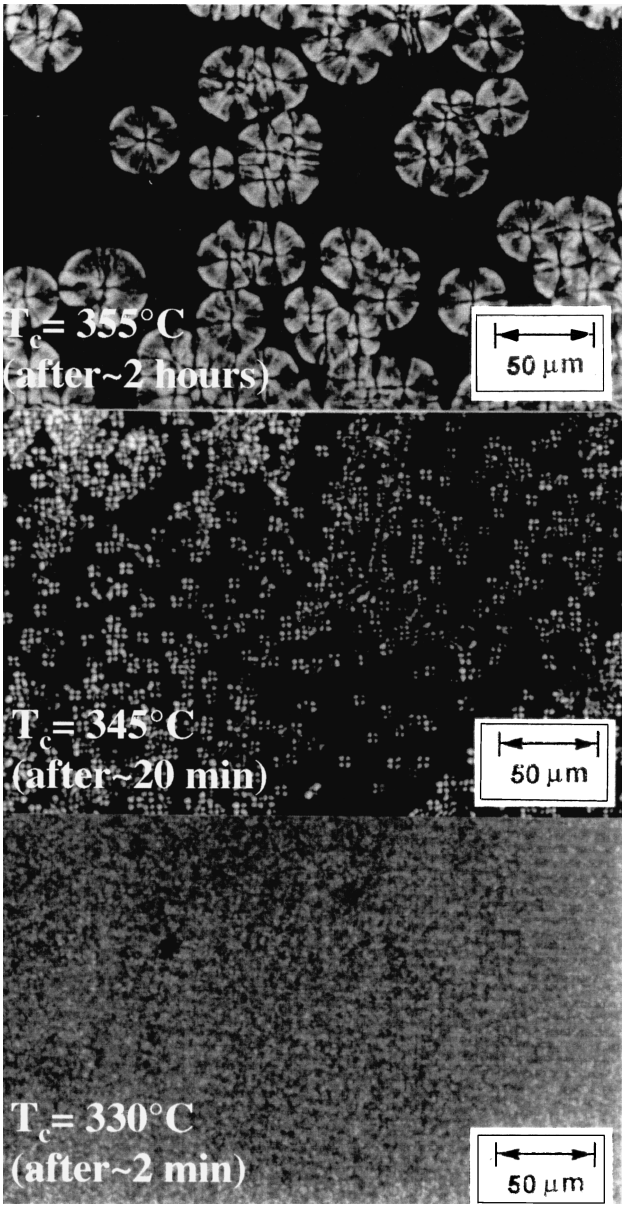

Fig. 4. Polarized optical micrographs at the indicated crystallization temperatures after being at a melt temperature of 430°C for 20 min.

earlier stages of crystallization where the presence of intermediate sheaf-like structures is more likely. These structures finally lead to a three-dimensional spherulite. However, these initial structures are not truly three-dimensional and thus would contribute to a decreased Avrami exponent [15,17]. Such an effect becomes even more important as the crystallization temperature is lowered and the nucleation density increases. This increase in nucleation density would result in a large number of only partially developed spherulites colliding with each other at an early stage thus giving rise to sheaf-like structures and/or truncated spherulites. This type of geometry would again lower the Avrami exponent.

3.1. Bulk crystallization rate, K

In order to compare the bulk crystallization rate of this polyimide with other high performance polymers, the value of the constant K can be compared. Before any such exercise, however, it is important to recognize that the units of K depend on the value of the Avrami exponent n, and thus, it is more useful to compare the values of $K^{1/n}$. Secondly, the supercooling at which these comparisons are made need to be similar. Also, the initial melt conditions can substantially affect the crystallization rate at a given undercooling. The initial melt temperature, if below the equilibrium melting point, can often result in self-seeding nucleation and thus lead to a higher value of the transformation rate K. Thus in order to assess the differences in crystallization kinetics and make valid comparisons, it is essential that the initial melt temperatures for the two polymers are above their respective equilibrium melting points. Some, other factors like molecular weight and its distribution are also important although these cannot be always held constant when comparing results from different studies. In this regard, the results from the various investigations [16–20] and this work are presented in Table 1. The fast crystallization rate of this polyimide is illustrated in that even for harsh melt conditions of 430°C and 20 min, and for a lower undercooling of 70°C, the value of $K^{1/n}$ (though lower than PPS) exceeds that of PEEK, an aliphatic flexible polyimide, and New-TPI. Less harsh conditions in terms of a lower T_m or t_m result in still faster crystallization rate at the same undercooling, this feature being discussed later in this paper.

The bulk crystallization rate K depends upon the nucleation mode, nucleation density (N_o) and the growth rate of the individual crystalline moieties (G) [21]. To better control the crystallization kinetics, the individual effect of these factors on kinetics and how they vary with temperature needs to be understood. For this purpose, the spherulitic growth rates (G) at the various crystallization temperatures (Fig. 5) were measured (the melt conditions were kept similar at 430°C, 20 min). It was found that at a particular crystallization temperature, G was constant with time and that it increased with increasing supercooling. The higher value of G contributes to a faster crystallization response at larger supercooling and this is reflected in the higher values of K obtained at 345°C. The increase in N_o with increasing supercooling also contributes to a faster crystallization rate as is clearly revealed by optical microscopy. While the nucleation mode is primarily athermal at 360°C, new spherulites also appear with time at lower crystallization temperatures, indicating some degree of thermal nucleation. This mixed mode of nucleation does not allow for a convenient calculation of a numerical value of the N_o using a simple expression like Eq. (2) from the classical Avrami theory. It is meaningful to recognize that although the optical micrographs shown here suggest increasing N_o to be more important, small changes in G alone may significantly affect the bulk transformation rate. Both these values, N_o and G, along with

Table 1
Bulk crystallization rates for some polymers

Polymer	Previous melt temperature (°C)	Undercooling, ΔT_c (°C)	$K^{1/n}$ (min^{-1})	Source
PEEK ($T_m^o = 395$°C)	370	80	0.17	Lee and Porter [16]
	410	80	0.06	
	400	80	0.05	Cebe and Hong [17]
	400	87	0.22	
Aliphatic flexible polyimide		96	0.01	Heberer et al. [18]
New-TPI ($T_m^o = 406$°C)	410	121	0.04	Hsiao et al. [19]
PPS ($T_m^o = 312$°C)	320	70	0.71	Lopez and Wilkes [20]
TPER–BPDA ($T_m^o = 410$°C)	430 (20 min)	70	0.46	This study
	430 (20 min)	55	0.12	
	430 (10 min)	55	0.24	
	430 (2 min)	55	0.61	
	410 (20 min)	55	0.37	

nucleation mode and the Avrami exponent n(the growth rate is raised to power n), determine K. The relative effect of growth rate can, however, be evaluated by comparing G and $K^{1/n}$. If effects due to nucleation density were absent, than the transformation rate $K^{1/n}$ would scale proportionally with changes in growth rate G. To obtain such an estimate, the relative changes in values of $K^{1/n}$ and G are compared at two typical crystallization temperatures of 340 and 345°C (the value of the Avrami exponent n is ca. 2 in both cases). While it is found that the value of $K^{1/n}$ is ca. 82% more at 340°C than at 345°C, the growth rate of the spherulites G is only increased by 14% at 340°C. This clearly suggests a stronger contribution of nucleation density (versus G) in increasing the bulk transformation rate. This more quantitative deduction is also in accordance with the qualitative trend observed in the optical micrographs (Fig. 4).

It is often observed that the overall crystallization consists of two separate parts: the initial stages being indicative of a primary crystallization process while, at later times, a change to a lower slope is often ascribed to secondary crystallization. Relative to primary crystallization kinetics, secondary crystallization further tends to lower the Avrami exponent by at least an order of magnitude or more. For crystallization of TPER–BPDA–PA, these changes in slope are more prominent for higher crystallization temperatures. Also, this change in slope occurs after ca. 60–70% of

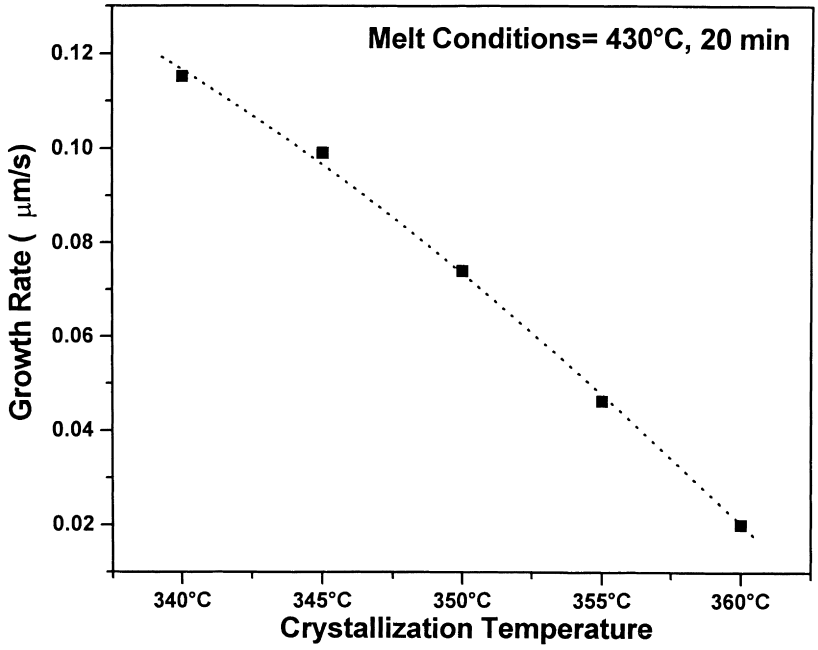

Fig. 5. Radial growth rates of spherulites at various crystallization temperatures after a melt temperature of 430°C for 20 min. ($M_n = 15,000$ Da, $M_w = 30,000$ Da).

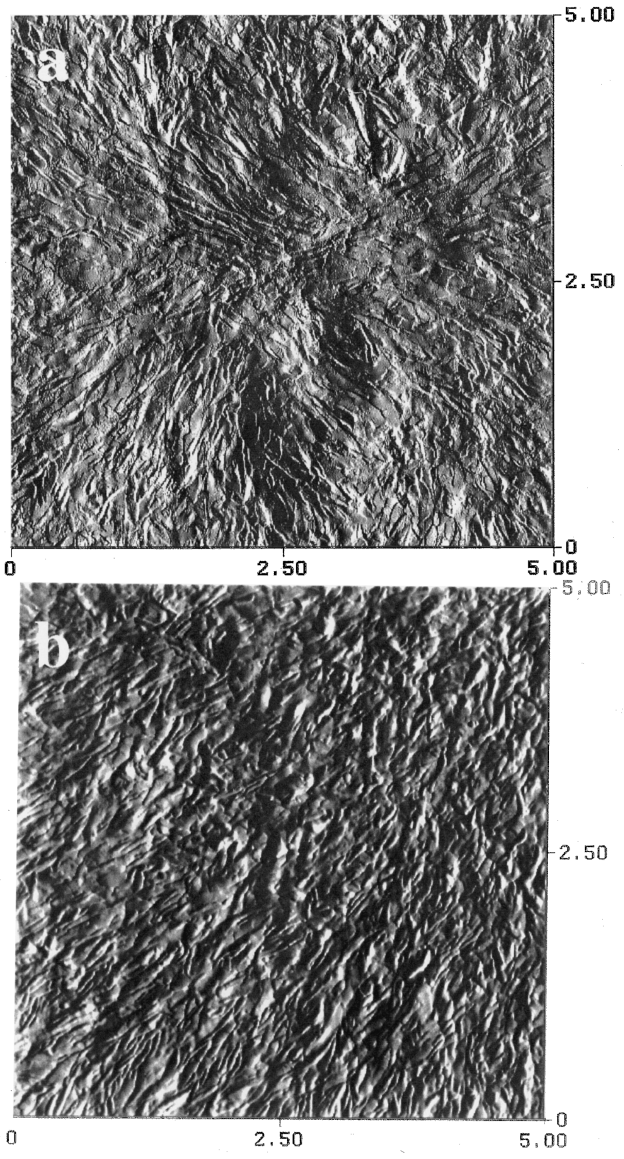

Fig. 6. (a) AFM height image of a central part of spherulite for a sample crystallized at 360°C after a melt temperature of 430°C for 20 min. (b) AFM height image of a outward region of a spherulite for a sample crystallized at 360°C after a melt temperature of 430°C for 20 min. The center of the spherulite lies toward the upper-right of the micrograph.

the total crystallization. The deviations from Avrami behavior at these conversions is also the reason for not using the crystallization half-time method [22] to calculate the two Avrami constants. Also in this case, the deviations in the slope always occur after the peak of the crystallization exotherm. It is often assumed that at times close to the peak, the likelihood of spherulitic collision in the bulk of the sample increases. Thus it is very likely that changes in slope are concurrently occurring with a large number of spherulitic collisions in the bulk sample, which will result in truncated spherulites. The effect of secondary crystallization will also be more visible after this time (as much of the primary crystallization has already taken place). Both these factors will contribute to a reduced slope. Such effects of secondary crystallization on the overall bulk crystallization kinetics have also been observed for numerous other polymers [23] including polyethylene [24,25], PEEK [11,12,26] and several other semicrystalline polyimides [13,14].

Although, the bulk morphology as revealed by optical microscopy is spherulitic, the underlying lamellar substructure responsible for such final spherulitic development is distinctly discernible by atomic force microscopy. Fig. 6(a) shows the AFM micrograph of a sheaf-like structure present at initial stages of development of a spherulite. Considerable branching of the lamellae in regions away from the center is observed which is finally responsible for a three-dimensional spherulitic structure. Fig. 6(b) shows the AFM micrograph of a region away from the center of a fully developed spherulite. Outwardly radiating lamellae from the center of the spherulite (the center of the spherulite is towards the bottom-right of the micrograph) are clearly revealed. It is particularly interesting that the fundamental crystalline structure of this polymer is lamellar although the polymer has a rather large repeat unit size ($M_u = 536$ Da). Also, earlier SAXS studies [3] in our laboratory have yielded an average Bragg spacing of ca. 163 Å for this polymer. Considerable twisting of the lamellae ('banding') could also be observed in our work, which is visible in the bottom-left section of the second AFM micrograph.

3.2. Effect of melt residence time (t_m) on crystallization kinetics

For such a high melting semicrystalline polyimide, the nucleation at any temperature can depend significantly on the melt processing temperature (T_m) and melt residence time (t_m). Even when the temperature is raised above the bulk melting point, the crystalline material present in the crevices and cracks of a heterogeneity may wet that surface and thus require a temperature above the bulk melting point for complete disordering [19,27,28]. These sites if not destroyed can serve as possible heterogeneous nucleation sites (nucleation due to residual nuclei) on subsequent cooling. The second type of nucleation that may affect the crystallization behavior is the self-seeding nucleation by crystals surviving the nominal melting point of the polymer [16]. To completely erase the effect due to this type of nucleation, it is often necessary to raise the temperature above the equilibrium melting temperature. The resulting nucleation density on cooling can thus be significantly dependent on the previous melt temperature and its position vis-a-vis the true equilibrium melting point of the polymer. Time in the melt is another important factor that might influence the subsequent crystallization. If exposed for very short amounts of time above the melting temperature, the crystals often reappear at exactly the same place (memory effect) [29]. Also, when the melt temperatures are in excess of 400°C, it becomes important to evaluate the effect of

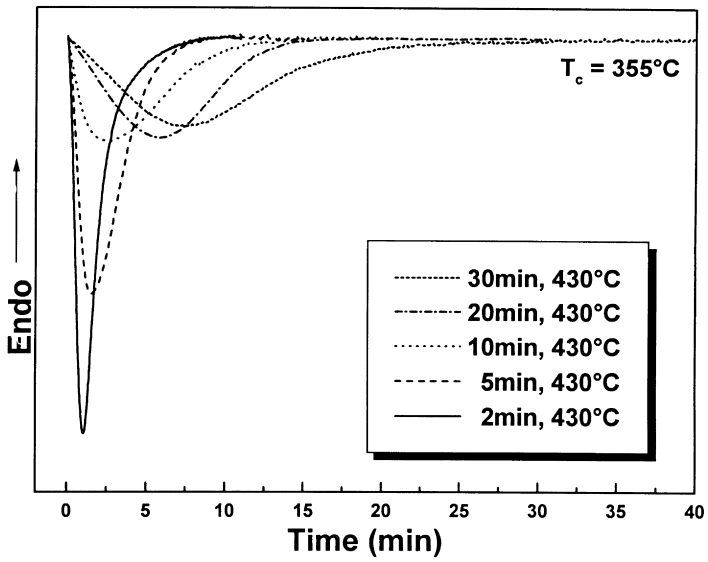

Fig. 7. Crystallization exotherms at 355°C after the various melt residence times at 430°C.

possible degradation reactions on the crystallization kinetics. Chemical changes leading to crosslinking, molecular weight increase or chain branching may inhibit the ability of the system to crystallize. The effect of such severe melt conditions on the crystallization kinetics thus serves as a direct tool in evaluating the thermal stability of the polymer.

For the above discussed reasons, the Avrami analysis was utilized to examine the effect of t_m and T_m on isothermal crystallization kinetics. For analyzing the effect of t_m, a typical melt temperature of 430°C (shown to be the optimum processing temperature for attaining the best adhesive strengths in an earlier work [4]) and a crystallization temperature of 355°C were selected. For such conditions, Fig. 7 illustrates the crystallization exotherms obtained after the t_m was varied between 2 and 30 min. It is clear that t_m has a major effect on the crystallization behavior of TPER–BPDA–PA. Short residence times of only 2 or 5 min result in a relatively faster crystallization response, while an increase in the t_m to 10 or 20 min leads to a significant decrease in the crystallization kinetics. For longer residence

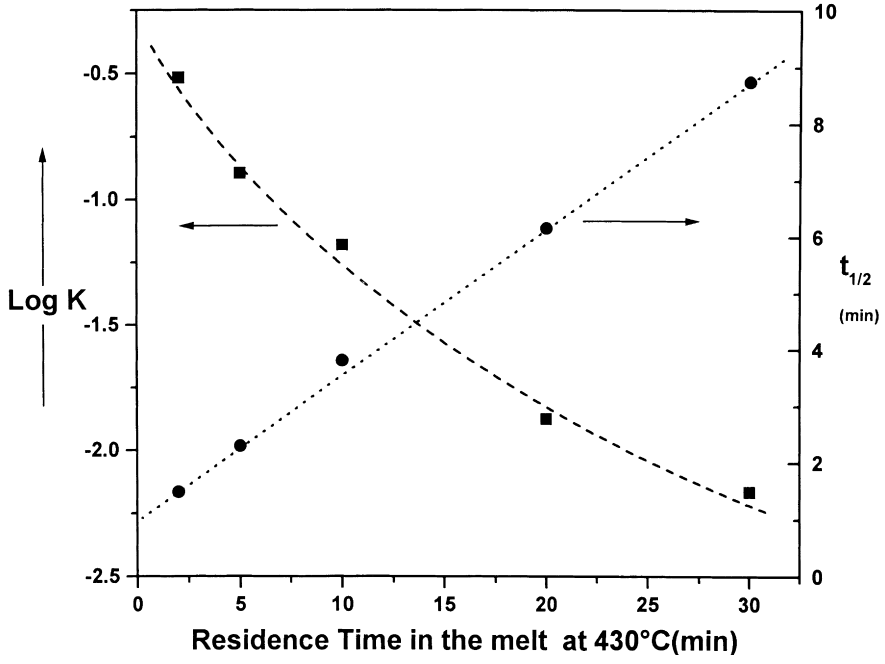

Fig. 8. Variation of the logarithm of transformation rate K and crystallization half time $t_{1/2}$ at a crystallization temperature of 355°C, as a function of residence time at 430°C.

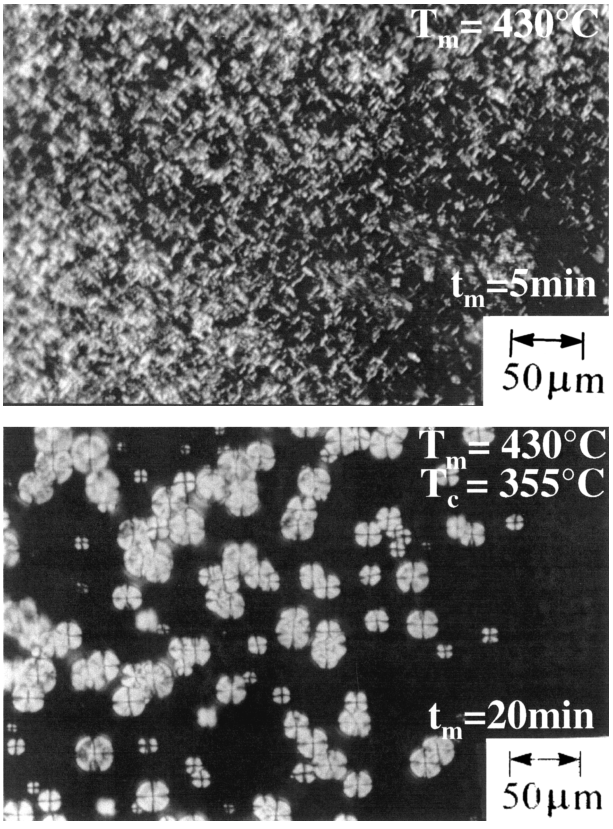

Fig. 9. Polarized optical micrographs at 355°C after the indicated melt residence times at 430°C.

time of 30 min, the decrease in crystallization rate is also accompanied by significant broadening of the crystallization exotherm. The corresponding Avrami plots (not shown) also show similar trends. However, the value of the Avrami exponent did not show much change ($n = 2.1$–2.4) with change in t_m. The value of K decreased progressively (Fig. 8) with increasing residence times in the melt, while $t_{1/2}$ showed a corresponding increase indicating again a slower rate of crystallization. The lower crystallization rate with increasing t_m can be due to the slower spherulitic growth and/or lower nucleation density. To examine this aspect, independent optical microscopy measurements were also conducted at the same crystallization temperature (Fig. 9). The optical micrographs reveal a significant drop in nucleation density with increased residence times in the melt at 430°C. For short residence times, the melt has not become truly homogenous and previous thermal history affects the subsequent crystallization. It is clear that a number of residual nuclei survive these short melt exposure times and serve as nucleation sites on cooling. However, with increasing melt exposure times, the melt becomes more homogenous and reduction in the number of surviving nuclei takes place, resulting in a lower nucleation density.

Later results presented in this paper show evidence of chemical changes occurring in the melt (including increases in the molecular weight through chain extension, branching and cross-linking) that tend to slow down the crystallization rate. These changes obviously increase for longer t_m. However, at shorter residence times of 2 and 5 min, where such degradation processes are minimal, the transformation rate K still shows a large decrease with only a small increase in t_m. To understand this behavior, the relative change in the values of G and $K^{1/n}$ were compared at two conditions. While the value of $K^{1/n}$ is 0.61 min^{-1} after a residence time of 2 min, it decreases to 0.40 min^{-1} by increasing the residence time to 5 min. The growth rates, however, are very similar for these conditions. This difference is thus clearly due to decreasing N_o for the higher '5 min' residence time. For still higher t_m, the degradation reactions that set in result in decreasing the spherulitic growth rates (shown later in Fig. 15), which then also contribute to slower crystallization kinetics. In this regard, $K^{1/n}$ decreases from 0.40 to 0.13 min^{-1} (i.e. by a factor of more than 3), as the t_m is increased from 5 to 20 min. The growth rate G also decreases by a factor of 2 for these conditions. Thus, at shorter t_m, variations in nucleation density are the primary factor influencing the crystallization kinetics. However, at longer t_m, the reduced spherulitic growth rates also contribute in decreasing the transformation rates.

3.3. Effect of melt temperature (T_m) on crystallization kinetics

The effect of melt temperature (T_m) on the crystallization kinetics is similar. Fig. 10(a) shows the crystallization exotherms at 355°C after cooling from T_m ranging from 410 to 430°C for 20 min. As the T_m is increased, the peak of the crystallization exotherm at 355°C shifts to longer times. While no considerable broadening is observed, the shapes of the crystallization exotherms change with increasing T_m. Interestingly, while the initial crystallization response markedly slows, the completion times for the overall crystallization do not show much change for the above range of T_m. The corresponding Avrami plot (Fig. 10(b)) shows the effect of increased melt temperatures on the Avrami constants K and n. K is significantly higher, while n also decreases by a magnitude of one, for lower T_m of 410°C. In this regard, optical micrographs (Fig. 11) at 355°C, after 20 min at the T_m of 420 and 440°C show a clear decrease in nucleation density for the higher T_m. The higher nucleation density will contribute significantly towards the higher values of the bulk crystallization rate K. The decrease in the growth rates with increasing T_m (discussed later in the paper) would also affect the bulk crystallization rates. Also, an increase in nucleation density leads to the development of more sheaf-like structures and thus a lower Avrami exponent.

Although most flexible chain polymers provide a sufficient temperature range above the melting point where such effects due to residual nuclei or self-seeding nucleation are greatly suppressed, similar results have been obtained for

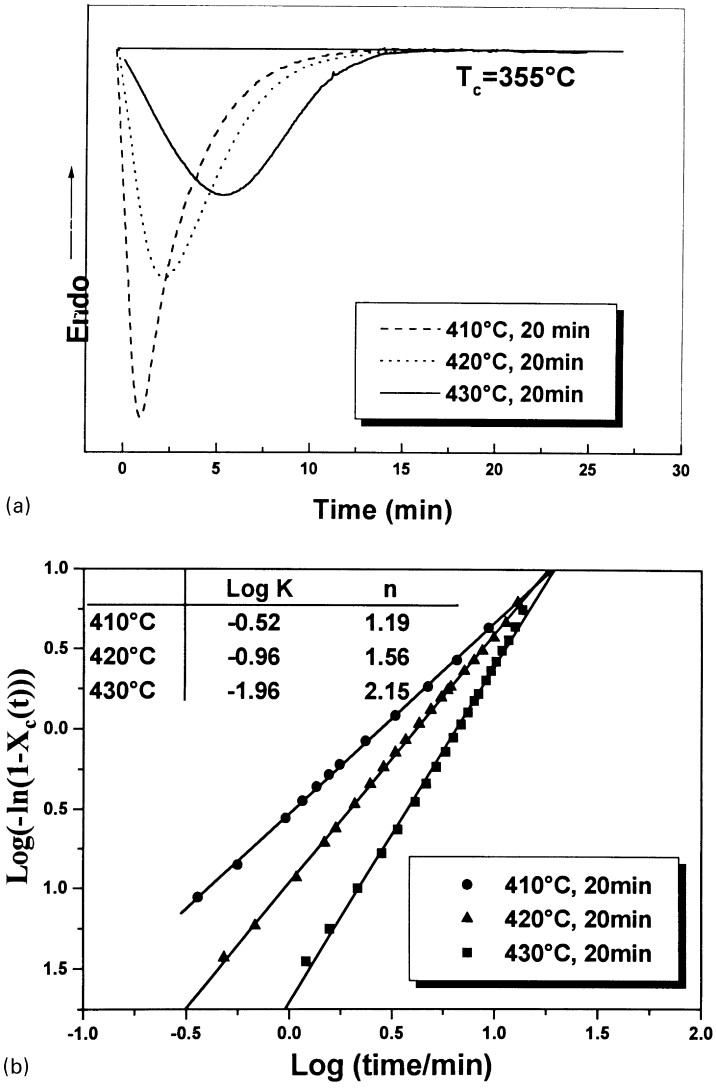

Fig. 10. (a) Crystallization exotherms at 355°C after a 20 min residence time at various melt temperatures. (b) Avrami plot of $\log[-ln(1 - X_c(t))]$ versus $\log(t)$ at 355°C after various melt temperatures and 20 min residence time.

other high melting polymers like PEEK [13,14,22]. Although higher t_m and higher T_m may be utilized to decrease the effect of previous thermal history, such conditions may also result in chemical reactions taking place. The ensuing discussion addresses this phenomenon.

4. Rheological studies

4.1. Isothermal frequency sweeps at 430°C

Depending on the chemical structure, semicrystalline semi-rigid chain polyimides, like the one utilized in this study, do not lend themselves to dissolution in any solvent and thus GPC analysis to quantify the initial molecular weight or the changes after the various melt treatments is not possible. However, melt viscosity determination at various times and temperature serves as a good qualitative tool to detect changes in the molecular weight due to chemical changes at the desired melt temperature. Also, any changes in viscosity are important from a melt-processing viewpoint. Fig. 12 shows the isothermal complex viscosity of TPER–BPDA–PA (15K) at 430°C as a function of frequency. The melt viscosity displays typical non-Newtonian behavior with the viscosity decreasing with increasing shear rates. At lower shear rates, the viscosity appears to be leveling off towards a constant value (zero shear viscosity). Owing to the times needed for data collection at various frequencies, the complex viscosity ($|\eta^*|$) at 0.1 Hz represents the values obtained after 8, 16, 24 and 32 min. It is very clear that the polymer is undergoing molecular weight changes at 430°C with the viscosity at the lower frequencies increasing by an order of magnitude within the time-frame of the experiment.

It is well known that η_0 often scales with M_w [3,4] for many linear polymers above the entanglement molecular

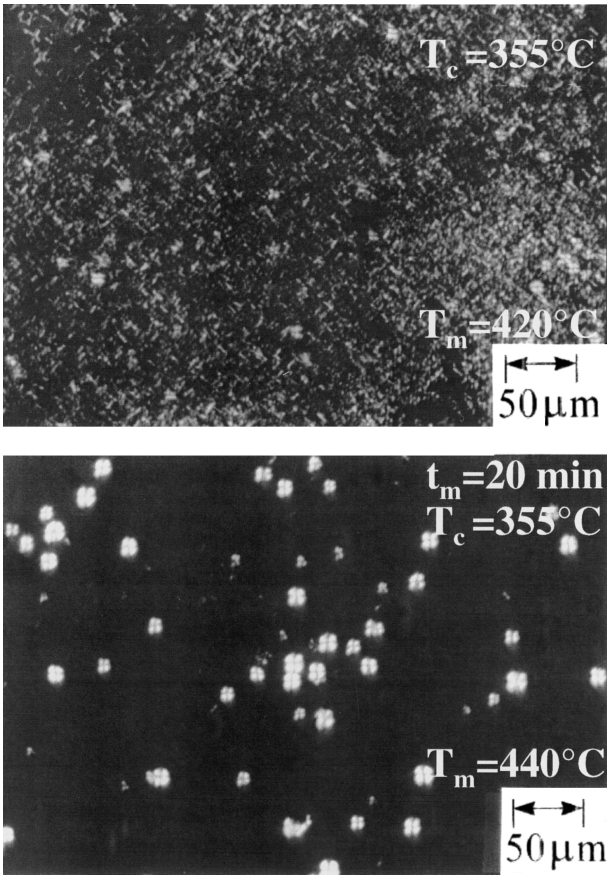

Fig. 11. Polarized optical micrographs at 355°C after the indicated melt temperatures and 20 min residence time.

weight. Thus assuming the initial M_w of ca. 30,000 Da (as determined by GPC analysis of the poly (amic acid)) to be above the entanglement M_w, this enables us to correlate the initial zero shear rate viscosity with M_w. In order to obtain a 'qualitative' evaluation of molecular weight changes occurring in the material with time at 430°C, calculation of η_0 is thus required for the different curves. To estimate these variations in η_0, the Carreau–Yasuda model was utilized to fit the experimental data. This five-parameter empirical model has proven very useful in the case of numerous polymer melts for providing analytical expressions for the non-Newtonian viscosity behavior and to estimate the value of η_0 from the available data which otherwise is often limited to the experimental window of attainable deformation rates. The model is given by the equation:

$$(\eta - \eta_\infty)/(\eta_0 - \eta_\infty) = [1 + (\lambda\gamma)^a]^{(n-1)/a} \quad (5)$$

Here λ is a characteristic 'time constant', n the power-law exponent and a a dimension-less parameter that describes the transition breadth from the zero shear-rate region to the power law region [30]. η_0 and η_∞ represent the zero-shear rate and infinite-shear rate viscosity, respectively. Also, for higher shear rates (100 rad/s); $\eta_\infty \ll \eta_0$ and thus η_∞ can be set equal to zero without introducing any significant error, though resulting in a simpler equation for fitting the data. While various values of a were tried, good fits of the data were obtained for $a = 2$. The calculated values of η_0 are indicated in Fig. 12. While the estimated value of η_0 is ca. 2900 Pa s after 8 min, it increases to ca. 55,000 Pa s after 32 min in the melt at 430°C. Before using these estimates of η_0 in the $\eta_0 \propto M_w$ [3,4] relationship, however, it needs to be realized that this relation holds strictly for linear polymers while some branching reactions are expected to occur

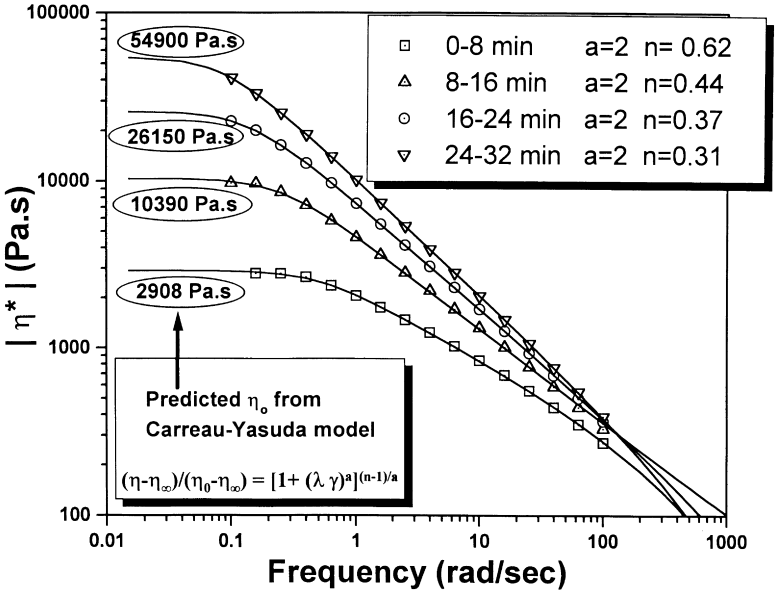

Fig. 12. Non-Newtonian viscosity–frequency profile of TPER–BPDA–PA (initial $M_n = 15,000$ Da, $M_w = 30,000$ Da) at 430°C. The plot also indicates the data collection times for consecutive scans at the same temperature.

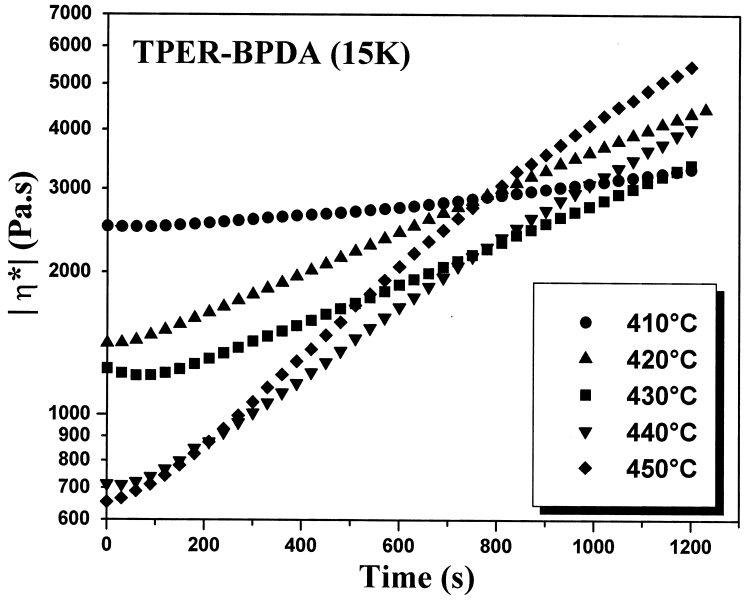

Fig. 13. Isothermal complex viscosity (1 rad/s) as a function of residence time in the melt at various melt temperatures.

for the present system at high melt temperatures. Thus its use here only gives a coarse estimate of the molecular weight changes occurring at harsh melt temperatures. This leads to the conclusion, that the initial weight-average molecular weight (M_w) of ca. 30,000 reaches ca. 44,000 after 16 min, ca. 57,000 after 24 min and ca. 71,000 after 32 min. These crudely estimated values indicate a more than two-fold increase in M_w after 32 min at 430°C. It is thus evident that while a process time of 20 min at 430°C was sufficient in our earlier adhesive study, relatively longer residence times of ca. 32 min at 430°C can lead to significant occurrence of chemical reactions resulting in build up of molecular weight.

4.2. Isothermal time sweeps at various melt temperatures

Fig. 13 shows the magnitude of the isothermal complex viscosity ($|\eta^*|$) at temperatures ranging from 410 to 450°C while keeping the frequency fixed at 1 rad/s. It is observed that the initial viscosity of the material is very sensitive to melt temperature. While the initial viscosity is ca. 2500 Pa s at 410°C, it decreases to ca. 650 Pa s when measured at 450°C. Firstly, the higher temperatures are expected to lead to a lower viscosity. Also, based on the previous microscopy experiments, it is known that although a large number of nuclei survive for 20 min at 410°C, even a short exposure at 440°C is able to greatly decrease this number. It is conjectured that this destruction of residual nuclei at higher temperatures, leading to a more homogenous melt, will contribute to lowering the viscosity. However, it is clear that chemical (degradation) reactions begin to influence the data at temperatures of 420 and 430°C since the viscosity begins to rise soon after the melting of the polymer. The difference in severity of these reactions at 420 and 430°C, however, is not great, as can be seen by the nearly parallel slope of viscosity versus time curves for the two temperatures. The small difference in viscosity curves at these temperatures may be attributed to both the differences in temperatures and to the difference in the population of residual nuclei. At 430°C, the viscosity (at 1 rad/s) increases from ca. 1200 Pa s to above 3000 Pa s within 20 min, which, as shown earlier, is indicative of branching/crosslinking (degradation). Interestingly however, earlier DSC studies [3,4] from our laboratories have shown that the melting behavior after similar melt treatment remains unaffected, with no changes in the peak melting point, heat of melting or broadness of the melting endotherm. Hence it is clear that although these changes in the magnitude of complex viscosity indicate some chemical changes, the overall crystallizability and melting behavior of the polymer show little change.

The degradation reactions at 440 and 450°C are significantly greater and lead to a faster increase in viscosity than at 420 and 430°C. Interestingly, for melt temperatures of 420 and 440°C, the final viscosity after a period of 20 min is nearly the same although the condition or structure of the melt is very different. While there is significantly less chemical reactions at 420°C, the lower temperature and the existing order in the melt are responsible for a higher viscosity. For a melt temperature of 440°C, however, the melt has an increased molecular weight due to crosslinking/chain branching while most of the residual order is completely destroyed. The slope of complex viscosity versus time can be approximately taken as the measure of the rate of degradation reactions at various temperatures. It is clear that the rate of chemical changes, although very similar at 420 and 430°C, is largely increased when the melt temperature is increased to 440 and 450°C. In fact,

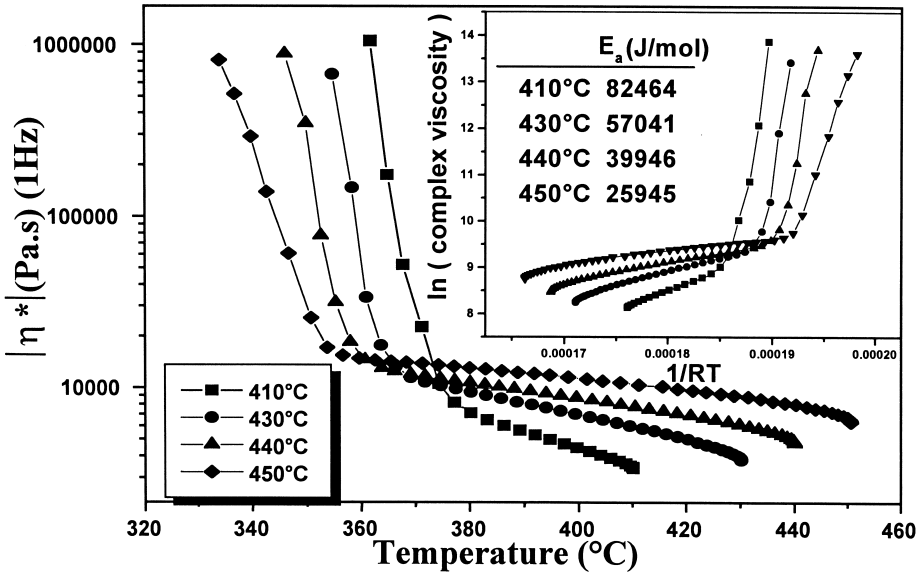

Fig. 14. Non-isothermal complex viscosity (1 rad/s) when cooled at 10°C/min from various melt temperatures after 20 min residence time. Inserted plot: corresponding Arrhenius plots for the non-isothermal viscosity profiles when cooled from the various melt temperatures. The initial regions prior to crystallization were utilized for estimating the activation energy using the Andrade–Eyring equation.

the viscosity increases by nearly an order of magnitude in 20 min at 450°C. Although the time-frame of 20 min was selected on the basis of our earlier work, it is noticed that the state of the melt would be very different for shorter holding times. For holding times shorter than 3 min at 450°C, a lower viscosity is achieved due to relatively little branching/crosslinking and a higher temperature. This lower viscosity will affect the melt processing as well as the final crystallization behavior on cooling.

4.3. Complex viscosity on cooling from various melt temperatures

For processing operations it is important to know the variation of melt viscosity with cooling and also the temperatures at which solidification of the melt due to the crystallization may occur. The effect of thermal history on solidification temperatures is thus examined when the polymer melt was cooled at 10°C/min after 20 min at various melt temperatures (Fig. 14). The onset of crystallization was observed for all samples with the viscosity increasing sharply at various degrees of supercoolings. A strong dependence, however, of the prior melt temperature on the crystallization is observed with the degree of supercooling necessary for crystallization increasing with higher melt temperatures. Lower melt temperatures hasten the onset of crystallization with the onset temperature shifting from 377 to 356°C when the melt temperature was changed from 410 to 450°C. Crystallization at such low supercooling, when cooling from 410°C, clearly shows the strong effect of residual nuclei on crystallization behavior. Also, the supercooling required for crystallization was ca. 7–8°C more for a sample cooled from 450°C in comparison to a sample cooled from 440°C. This difference cannot be attributed to the residual nuclei, as there is little difference in their population at these two temperatures. However, the higher molecular weight of samples caused by higher melt temperature leads to slower crystallization. Both the decreasing population of residual nuclei with increasing melt temperatures as well as the increased molecular weight of samples exposed to higher melt temperatures contribute to the onset temperature of crystallization. However, it should be clear that there is a frequency dependence in the above analysis and thus only qualitative trends can be made. For the same reason these results cannot be quantitatively compared with traditional DSC experiments, which are less sensitive in detecting the onset of crystallization.

4.4. Activation energy (E_a) values on cooling from various melt temperatures

It was also noted that the viscosity profiles before the onset of crystallization were also dependent upon the previous thermal history. It is well established that, the viscosity dependence on temperature can generally be described by the Andrade–Eyring equation [31]:

$$\eta = B \exp(E_a/RT) \tag{6}$$

This equation was derived initially for small molecules and is generally valid at temperatures in excess of 100 K above T_g for amorphous polymers. Here E_a is the flow activation energy of viscous flow and is representative of the energy barrier for successive segmental jumps into unoccupied sites or 'holes'. The value of E_a thus depends on the ease with which the polymer segments can 'jump' into the available holes [32]. The lower 'jump frequency' (higher E_a) can

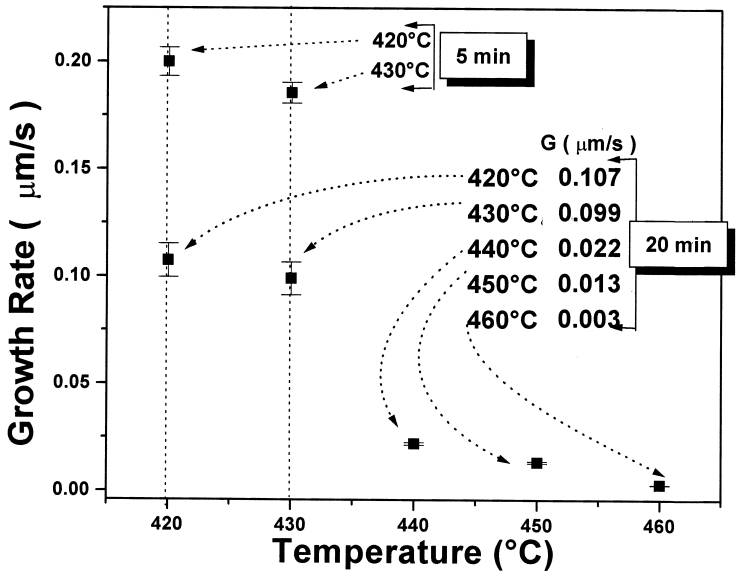

Fig. 15. Spherulitic growth rates at 345°C after 20 min at various initial melt temperatures.

also be viewed as the result of a higher degree of co-operativity needed to create the required 'holes'. The value of E_a varies between 20 KJ/mol to well over 120 KJ/mol for various polymers. The inset in Fig. 14 also shows the corresponding Arrhenius plots based on this relationship. The regions of the curve before the onset of crystallization were used to estimate the activation energy for different curves. The activation energy was found to depend strongly on the initial thermal history. While the value of activation energy obtained was 82 KJ/mol when cooled from 410°C, it was only 26 KJ/mol when cooled from a melt temperature of 450°C. It is well recognized that 'local segmental character' and not the molecular weight determines the value of activation energy. The value of activation energy, although dependent upon the chemistry, can also differ with changes in chain topology. Long-chain branched polymer would be expected to show a higher value of activation energy than its linear homologue, the difference being dependent upon the amount and nature of the branching [33,34]. In this regard, the increase in molecular weight for a higher melt temperature would not contribute to the values of activation energy obtained. However, the branching reactions that occur at these higher temperatures, would only serve to increase the rotational restrictions along the chain backbone and thus should lead to a higher value of activation energy. However, an opposite trend is observed here. This result can be explained on the basis of residual nuclei that become destroyed only at higher T_m. This leads to a more homogenous melt, and thus a substantially lower value of activation energy at higher T_m. However, this homogeneity at higher T_m is accompanied with increased viscosity and higher molecular weight. It should be mentioned that evaluation of E_a would show some frequency dependence if such an analysis is carried out in the shear-thinning region. In this case, however, results are based on viscosity at 1 rad/s, the lowest frequency experimentally feasible for such a study. The values of E_a thus obtained serve more as a comparison between various experimental conditions rather than suggesting some truly absolute value for the polymer.

4.5. Growth rates as a function of melt histories and non-isothermal behavior

It has now been demonstrated that harsher melt conditions lead to slower crystallization kinetics, which is in part due to the reduction in residual nuclei. Another important reason for slower crystallization response may be the decreased spherulitic growth rates due to increased melt viscosity (enhanced molecular weight) after harsher melt conditions. To evaluate this effect, thin polymer films sandwiched between two glass slides were quenched to 345°C after 20 min at 420–460°C. Interestingly, a spherulitic morphology was observed even after 20 min in the melt at 460°C. This perhaps is the highest melt temperature from which organic polymer spherulites have been observed on cooling after such a long residence time in the melt. However, both higher values of T_m and t_m, which were shown to result in increased degradation (branching) reactions, are also associated with significantly reduced growth rates (Fig. 15). Thus results from independent microscopy and rheology experiments are in concurrence.

For a t_m of 20 min, the growth rates, although similar at 420 and 430°C, show a sharp decrease if the T_m is raised above 430°C. This indicates that the extent of branching/cross-linking reactions is largely increased if the melt temperatures are taken above 430°C. However, growth rates after 5 min at 420 and 430°C are almost twice as fast than when t_m is 20 min, thereby indicating that some chemical changes do even occur at 420 and 430°C. A similar conclusion was also reached after the previous rheological

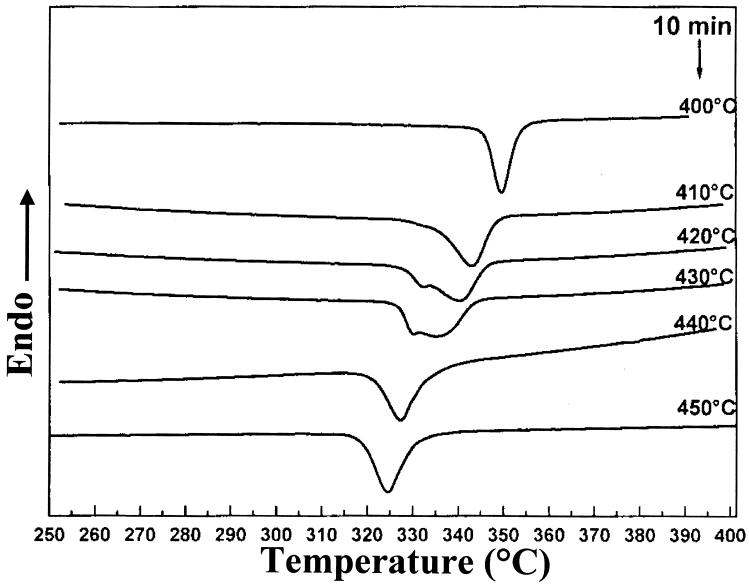

Fig. 16. DSC cooling scans at 10°C/min after 20 min at various melt temperatures.

study and in our earlier papers [3,4]. These conclusions also highlight the importance of melt conditions for studies dealing with other high melting polymers. Proper selection of initial melt conditions is vitally important before any fundamental studies are attempted to model the crystallization behavior. However, for many such polymers including the one utilized in this study, such ideal conditions may not exist.

The above spherulitic growth-rate study also has important ramifications with regards to more conventional non-isothermal crystallization behavior, as seen typically in the melt processing operations. These results indicate that for a given cooling rate, as the initial melt temperature is increased, the crystallization would occur at larger supercooling. In fact, for harsher melt conditions, for e.g. 460°C for 20 min, the growth rates are significantly reduced and thus it should be possible to quench the polymer to a state with little or no crystallinity present. However, for such a sample that was quenched from a melt at 460°C for 20 min, a significant amount of crystallinity was found to be present by DSC and a very fine grainy morphology was revealed by optical microscopy. Non-isothermal studies were thus attempted to interpret this behavior.

4.6. Evidence of catastrophic nucleation

DSC was utilized to observe the non-isothermal crystallization behavior from different initial melt temperatures. Fig. 16 shows the cooling scans at 10°C/min after 10 min in the melt at temperatures varying from 400 to 450°C. As the temperature is increased beyond 400°C, the crystallization exotherm shifts to higher undercoolings, the degree of shift increasing with increasing T_m. While the scans from 400 and 450°C give a characteristic single crystallization peak, the intermediate scans lead to a double peak in the crystallization exotherm. The sharper (and higher) crystallization exotherm (from 400°C) is believed to result from the recrystallization of previously unmelted residual crystals. However, it is interesting to note that a second crystallization peak appears for intermediate T_m. This second peak appears first as a shoulder on the low temperature side of the exotherm when cooling from 410°C, but becomes a separate peak as the T_m is increased. It is clear that this double exothermic behavior is indicative of two separate crystallization phenomena. The occurrence of these crystallization exotherms, however, is dependent on previous melt history. Also, earlier studies [4,5] have not indicated any evidence of polymorphism in this polymer.

Isothermal crystallization experiments were performed at temperatures in the vicinity of the double exothermic behavior (at 335°C) using a hot-stage POM. It was found that the initial spherulitic crystallization was followed by a sudden 'catastrophic nucleation' leading to the development of a fine grainy background. The details of the superstructure that developed due to this catastrophic nucleation were not optically resolvable and caused the initially observable larger spherulites to become totally enveloped in the subsequent overall fine pattern. The double exothermic behavior on non-isothermal crystallization from the melt is easily explained due to this catastrophic nucleation process. When cooling from 420°C, the initial exotherm is indicative of spherulitic development, while the onset of 'catastrophic nucleation' at lower temperatures leads to a second exothermic peak. As shown earlier, increasing the melt temperature to 440 and 450°C leads to a significant reduction in the nucleation density (Fig. 11) and much decreased spherulitic growth rates (Fig. 15). Thus, a lesser number of heterogeneous sites available for spherulitic development and reduced spherulitic growth rates decrease the chances of any spherulitic crystallization at lower supercooling (i.e.

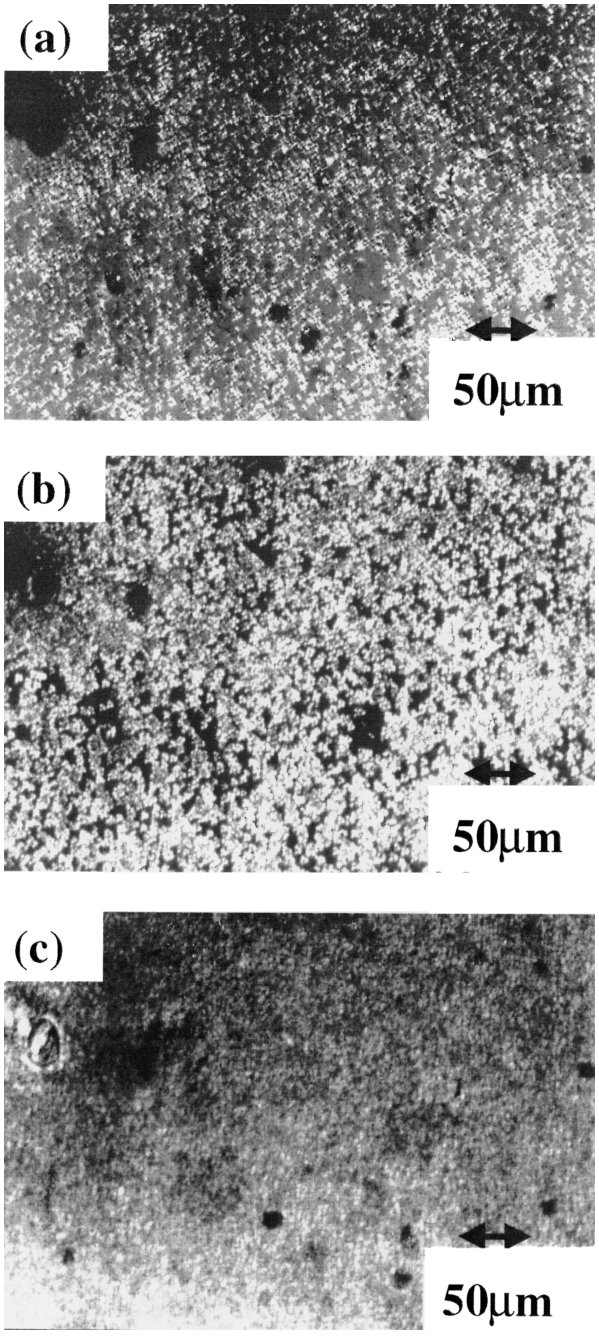

Fig. 17. Polarized optical micrographs illustrating the morphological development when cooled at 20°C/min from the melt at 430°C for 20 min. Micrographs taken at: (a) 340°C; (b) 332°C; and (c) 323°C.

at $T_c > 340$°C) during a non-isothermal cooling scan in a DSC. This is indeed clearly observed in DSC cooling scans (Fig. 16) as the melt temperatures are increased to 440 and 450°C. While at temperatures lower than 430°C, initial spherulitic crystallization contributes significantly to the overall crystallization, the second 'catastrophic nucleation' process is mainly responsible for crystallization from 440 and 450°C. The crystallization peak, however, shifts to 324 from 327°C as the melt temperature is increased from 440 to 450°C, thus indicating a small dependence of 'catastrophic nucleation' on the initial melt temperature.

To study the crystalline morphology when crystallization occurs under non-isothermal conditions, a typical experiment was performed from the melt (430°C, 20 min) at a cooling rate of 20°C/min. While spherulitic development begins early, a subsequent decrease in the temperature in the vicinity of 330°C leads to a catastrophic increase in nucleation density as shown in the last micrograph of Fig. 17. As also observed in separate isothermal experiments, this rapid increase in nucleation density leads to the development of a fine pattern, which envelops the initially growing spherulites. However when cooled from higher melt temperatures (e.g. 450°C), at the same cooling rate, no spherulites were observed, and only the 'catastrophic nucleation' was responsible for the crystallization. The initial melt conditions and cooling rate thus are critical in deciding the final morphology of this polymer.

5. Conclusions

Isothermal crystallization of a new semicrystalline polyimide, TPER–BPDA–PA was characterized as a function of crystallization temperature and thermal history in the melt. It was found that isothermal crystallization was very sensitive to crystallization temperature thereby limiting the thermal window of study. The holding time in the melt also had a strong affect on crystallization behavior. At a given supercooling, increased holding time in the melt at 430°C substantially broadened the crystallization exotherm. While the Avrami exponent did not show a significant change, the value of the Avrami parameter K decreased considerably with the residence time in the melt. Melt temperatures also affected the crystallization behavior substantially with the Avrami analysis showing strong changes in both the exponent n and the parameter K. A substantial decrease in the nucleation density with harsher melt conditions was revealed by optical microscopy and was primarily responsible for slowing the crystallization kinetics at 355°C.

Melt viscosity experiments showed the presence of chemical reactions (branching/cross-linking) at 430°C. The rate of these reactions however, increased substantially above 440°C, while it was distinctly slower below 430°C. Although a higher T_m and a longer t_m leads to an enhanced molecular weight, higher values of each these variables helps to remove the previous thermal history to a large extent. Crystallization experiments (by rheometery) showed that the onset of crystallization shifts to higher undercoolings with increasing T_m. The estimated activation energies decreased strongly with increasing melt temperatures, thus indicating the prevalence of residual order in the melt till high T_m.

Isothermal experiments at 345°C showed that growth rates were also dependent upon the previous T_m, with large decreases in growth rates observed for T_m above

430°C. The growth rates, though similar at 420 and 430°C, did show a significant effect of t_m, with shorter residence times leading to higher growth rates due to lesser degradation. Interestingly, spherulites (with no observable change in the overall superstructure) were even obtained from melt temperatures as high as 460°C after residence times as long as 20 min. Non-isothermal DSC experiments revealed double peaks in the crystallization exotherms. A 'catastrophic nucleation' process was found to explain the presence of the second peak, as revealed by both isothermal and non-isothermal POM studies. This second crystallization process dominated the overall crystallization as the melt temperatures were raised. The crystalline morphology resulting from this 'catastrophic nucleation' process could not be resolved by optical microscopy.

Acknowledgements

The authors wish to thank the NSF Science and Technology Center for High Performance Polymeric Adhesives and Composites for full support of this study under contract number DMR 9120004. Generous support from the GenCorp Foundation is also acknowledged.

References

[1] Hergenrother PM, Stenzenberger HD, Wilson D. Polyimides. London: Blackie, 1990.
[2] Mittal KL, Ghosh MK. Polyimides: fundamentals and applications. New York: Marcel Dekker, 1996.
[3] Wilkes GL. Encyclopedia of Physics and Science Technology 1987;11:61.
[4] Ratta V, Stancik EJ, Ayambem A, Parvatareddy H, McGrath JE, Wilkes GL. Polymer 1999;40:1889.
[5] Srinivas S, Caputo FE, Graham M, Gardner S, Davis RM, McGrath JE, Wilkes GL. Macromolecules 1997;30:1012.
[6] Sasuga T. Polymer 1991;32:1539.
[7] Chang AC, Hou TH, St. Clair, TL. Polyimides: trends in materials and applications. In: Proceedings of the Fifth International Conference on Polyimides. 1994. p. 3.
[8] Graham MJ, Srinivas S, Ayambem A, Ratta V, Wilkes GL, McGrath JE. Polymer Preprints. April 1997;38(1):306.
[9] Grenier D, Homme REP. Journal of Polymer Science: Polymer Physics Edition 1980;18:1655.
[10] Price FP. Journal of Applied Physics 1965;36:3014.
[11] Tomka J. European Polymer Journal 1968;4:237.
[12] Hillier IH. Journal of Polymer Science: Part A 1965;3:3067.
[13] Banks W, Hay JN, Sharples A, Thompson G. Polymer 1964;5:163.
[14] Hsiao BS, Kreuz JA, Cheng SZD. Macromolecules 1996;29:135.
[15] Muellerleile JT, Risch BG, Rodrigues DE, Wilkes GL. Polymer 1993;34:789.
[16] Lee Y, Porter RS. Macromolecules 1988;21:2770.
[17] Cebe P, Hong S. Polymer 1986;27:1183.
[18] Heberer DP, Cheng SZD, Barley JS, Lien SHS, Bryant RG, Harris FW. Macromolecules 1890:24.
[19] Hsiao BS, Sauer BB, Biswas A. Journal of Polymer Science: Part B: Polymer Physics 1994;32:737.
[20] Lopez LC, Wilkes GL. Polymer 1988;29:106.
[21] Wunderlich B. Macromolecular physics: crystal nucleation, growth and annealing, vol. 2. New York: Academic Press, 1976.
[22] Risch BG, Warakomski JM, Wilkes GL. Polymer 1993;34:2330.
[23] Fatou JG. Crystallization kinetics. Encyclopedia of polymer science and engineering, New York: Wiley, 1989. p. 231 (supplementary volume).
[24] Hoffman JD, Davis GT, Lauritzen Jr. JI. In: Hannay HB, editor. Treatise in solid-state chemistry, vol. 3. New York: Plenum Press, 1976. p. 497.
[25] Ergoz E, Fatou JG, Mandelkern L. Macromolecules 1972;5:147.
[26] Jonas A, Legras R. Polymer 1991;32:2691.
[27] Turnbull D. Journal of Chemical Physics 1950;18:198.
[28] Morgan LB. Journal of Applied Chemistry 1954;4:160.
[29] Jorda R, Wilkes GL. Polymer Bulletin 1988;19:409.
[30] Bird RB, Armstrong RC, Hassager O. Dynamics of polymeric liquids, Fluid mechanics, vol. 1. New York: Wiley, 1987. p. 171.
[31] Mendelson R. Polymer Engineering Science 1968;8:235.
[32] Cowie JMG. Polymers: chemistry and physics of modern materials, 2nd ed.. London: Blackie, 1997. p. 255.
[33] Wilkes GL. Journal of Chemical Education 1981;58:880.
[34] Janzen J, Colby RH. Journal of Molecular Structure 1999;569:485.